Applied Catalysis A: General 407 (2011) 91–99

Contents lists available at SciVerse ScienceDirect

Applied Catalysis A: General

journal homepage: www.elsevier.com/locate/apcata

Hydrogen spillover behavior of Zn/HZSM-5 showing catalytically active protonic acid sites in the isomerization of *n*-pentane

Sugeng Triwahyono[a,*], Aishah Abdul Jalil[b], Rino R. Mukti[c], Malik Musthofa[a], N. Aini M. Razali[b], M. Arif A. Aziz[b]

[a] *Ibnu Sina Institute for Fundamental Science Studies, Faculty of Science, Universiti Teknologi Malaysia, 81310 UTM Johor Bahru, Johor, Malaysia*
[b] *Department of Chemical Engineering, Faculty of Chemical Engineering, Universiti Teknologi Malaysia, 81310 UTM Johor Bahru, Johor, Malaysia*
[c] *Division of Inorganic and Physical Chemistry, Faculty of Mathematics and Natural Sciences, Institut Teknologi Bandung, Jl. Ganesha 10, Bandung 40132, Indonesia*

ARTICLE INFO

Article history:
Received 23 May 2011
Received in revised form 12 August 2011
Accepted 17 August 2011
Available online 24 August 2011

Keywords:
Zn/HZSM-5
Protonic acid sites
Lewis acid sites
Molecular hydrogen
n-Pentane isomerization

ABSTRACT

The impregnation of zinc particles into MFI zeolite (HZSM-5) caused the formation of catalytically active protonic acid sites for isomerizing *n*-pentane in the presence of hydrogen. An infrared (IR) study with preadsorbed pyridine revealed that these protonic acid sites originated from the spillover of molecular hydrogen from the zinc species onto the zeolite surface. The requirements for this spillover effect were further studied by IR spectroscopy of adsorbed ammonia and carbon monoxide. The presence of zinc species in HZSM-5 suggested the exchange of acidic character towards strong Lewis acids rather than Brønsted acid sites. The isomerization of *n*-pentane over the Zn/HZSM-5 catalyst resulted in high activity and stability and the conversion to *iso*-pentane depends on the promotive effect of hydrogen as a carrier gas.

1. Introduction

The isomerization of light paraffins such as *n*-pentane, *n*-hexane and *n*-heptane proceeds via hydrogen dissociation on a metal under a hydrogen atmosphere along with the occurrence of hydrocracking side reactions [1,2]. The promotive effect of hydrogen on the high isomerization activity, such as with Pt/SO_4^{2-}-ZrO_2 and Pt/WO_3-ZrO_2 catalysts, has been interpreted by the generation of protonic acid sites via which the hydrogen migrates or spillsovers from a noble metal site onto the acidic oxide support during the reaction [3–8]. In fact, this hydrogen spillover phenomenon has only been observed for a limited class of catalysts [9,10]. Due to the importance of acid-catalyzed alkane isomerization to achieve the high octane number of high-quality gasoline, further development of these kinds of solid acid catalysts that are stable, regenerable and active at low temperatures is necessary.

Solid acid catalysts such as alumina, zirconia, mesoporous silica and zeolites have been used as supports for promoting metals or noble metals due to their non-corrosive, high surface area and deactivation-free characteristics [11–16]. Bifunctional catalysts that consist of metallic and acidic components effectively promote the isomerization of alkanes [17–21]. However, a major drawback of using sulfur-based solids is their tendency to form volatile compounds and their intolerance against water poisoning during catalytic reactions, thus preventing the catalyst from being applicable and regenerated. Among those supports, zeolites are especially promising because these crystalline microporous materials are well known for their shape selectivity, good thermal stability, hydrophobicity and strong electron transfer to their enormous acid sites [22–25].

In the case of zeolites, the hydrogen spillover effect has been observed on zeolite-supported metals (bifunctional catalyst) and zeolite physically mixed with metals supported on silica (hybrid catalyst) [2,26–29]. In the presence of platinum as a promoter, the isomerization activity and selectivity of zeolites can be favored over the cracking activity [30]. In addition, the introduction of Zn species into HZSM-5 (medium-pore MFI-type zeolite) can be used to increase the rate and selectivity of other hydrocarbon conversions, such as aromatization reactions, by inhibiting the undesirable β-scission side reaction [31,32]. Nevertheless, the catalytic role of Zn species is controversial. The synergy between acid sites and exchanged cations during alkane activation have been described. In this work, we studied the hydrogen spillover effect of zinc particles impregnated into HZSM-5 (Zn/HZSM-5) and tested them in the isomerization of *n*-pentane. The crystal size has been found to be of paramount importance for advancing the molecular diffusion pathlength in catalysis [30]. Therefore, we used a Zn^{2+}/N,N-dimethylformamide solution to impregnate zinc

* Corresponding author. Tel.: +60 7 5536076; fax: +60 7 5536080.
E-mail address: sugeng@utm.my (S. Triwahyono).

0926-860X/$ – see front matter © 2011 Elsevier B.V. All rights reserved.
doi:10.1016/j.apcata.2011.08.027

particles with sizes ranging from 10 to 15 nm into the commercial zeolite.

Although many studies have used IR spectroscopy to investigate the hydrogen spillover effect [28,29], the requirement of a solid acid catalyst for this effect is not clear. We carefully examined the nature of zeolite acid sites before and after metal impregnation to understand the promotive effect of zinc particles in the presence of hydrogen. The spillover effect was monitored in detail by IR spectroscopy using pyridine as a molecular probe under a hydrogen atmosphere. The role of the zinc particles in zeolite was also studied with IR spectroscopy using carbon monoxide and ammonia adsorption. Based on these complementary IR characterizations, the requirement of the solid acid catalyst for a hydrogen spillover effect has been clarified. The formation of protonic acid sites catalyzes the isomerization of *n*-pentane.

2. Experimental

2.1. Preparation of catalyst

Commercial HZSM-5 (Zeolyst) with an Si/Al atomic ratio of 80 was used as a support for the zinc catalyst. This commercial zeolite contains only Brønsted acid sites after treatment at 773 K for 3 h [5]. The Zn^{2+}/N,N-dimethylformamide solution was used as the zinc particle precursor and was prepared following the procedures of Jalil et al. [33]. In brief, a N,N-dimethylformamide solution (Merck) containing naphthalene and tetraethylammonium perchlorate was added to one compartment of a cell equipped with a zinc plate (2 cm × 2 cm) as an anode and a platinum plate (2 cm × 2 cm) as a cathode. The electrodeposition of Zn^{2+} was then executed at 273 K. The Zn/HZSM-5 was prepared by impregnation of HZSM-5 with the Zn^{2+}/N,N-dimethylformamide solution at 353 K, followed by drying at 393 K overnight and calcining at 823 K for 3 h in the air. The amount of zinc particles was adjusted to 5 wt% in the catalyst.

2.2. Characterization of catalyst

The crystallinity of HZSM-5 and Zn/HZSM-5 was confirmed by X-ray diffraction (XRD) recorded on a powder diffractometer (40 kV, 40 mA) using a Cu Kα radiation source. While, X-ray photoelectron spectroscopy (XPS) of Zn/HZSM-5 was conducted on a Kratos Ultra spectrometer with MgKα radiation source (10 mA, 15 kV) and the XPS peaks are internally referenced to the binding energy of C (1s) peak at 284.5 ± 0.1 eV. The BET specific surface area was calculated from the adsorption data of N_2 adsorption–desorption isotherms at the relative pressure of 0.01–0.2 on a Quantachrome Autosorb-1 instrument. Prior to analysis, the sample was outgassed at 573 K for 3 h. For imaging of the zinc oxide particles, a powder form of the zinc oxide particles was obtained by separating the solid from Zn^{2+}/N,N-dimethylformamide solution by centrifugation at 20,000 rpm for 30 min. The solid was then dried at 393 K overnight and calcined at 823 K for 3 h in the air. The morphology and size of the zinc oxide particles in the powder form were observed using a transmission electron microscope (TEM). For the TEM observations of ZnO particle and Zn/HZSM-5 samples, a powder sample dissolved in hexane and dropped onto the copper grid. A field-emission scanning electron microscope equipped with an energy dispersion X-ray spectrometer (SEM-EDX) was used to observe the morphology as well as to obtain the elemental analysis of the sample. Before observation by SEM-EDX, the sample was coated by Pt using a sputtering instrument.

2.3. IR spectroscopy

IR spectroscopy of adsorbed pyridine was used to evaluate several types of acid sites such as Brønsted, Lewis or protonic sites as a result of the hydrogen spillover effect. In addition, ammonia and carbon monoxide were adsorbed to observe the acid strength. The IR spectra were recorded on a transmission spectrometer. The sample was prepared as a self-supporting wafer and activated under vacuum at 623 K for 3 h in accordance to Ref. [34]. The adsorption of pyridine (2 Torr) was conducted at 423 K for 30 min, followed by outgassing at 598 K for 30 min. For ammonia (5 Torr), the adsorption was conducted at 373 K for 30 min, followed by outgassing at 373 and 473 K for 30 min, respectively. The adsorption of carbon monoxide (2 Torr) was conducted at room temperature for 10 and 30 min. All spectra were recorded at room temperature. To compare the surface coverage of the adsorbed species between different wafer thicknesses, all spectra were normalized using the overtone and combination vibrations of the MFI between 2105 and 1740 cm^{-1} after activation [35–37].

To study the generation and elimination of protonic acid sites formed after introducing hydrogen molecules on the catalyst, the pyridine-adsorbed catalyst was exposed to 50 Torr of hydrogen at room temperature. The catalyst was then heated stepwise from room temperature to 398 K with heating increments of 25 K. To remove the hydrogen, the catalyst was outgassed by stepwise heating from 323 to 573 K with heating increments of 50 K.

2.4. Isomerization of n-pentane

Isomerization of *n*-pentane was performed on a microcatalytic pulse reactor at 523 K. Initially, the catalyst was treated in an oxygen stream (F_{Oxygen} = 100 ml/min) for 1 h followed by hydrogen stream ($F_{Hydrogen}$ = 100 ml/min) for 3 h at 673 K and then cooled down to reaction temperature of 523 K. A dose of *n*-pentane (43 μmol) then was passed over 0.3 g of activated catalyst, and the products were trapped at 77 K before flash-evaporation into an online 6090N Agilent gas chromatograph equipped with a VZ-7 packed column and FID detector. The intervals between each dose were kept constant at 30 min.

The selectivity for a specific product (S_i) was calculated according to Eq. (1)

$$S_i = \frac{c_i}{c_1 + c_2 + c_3 + c_4 + ic_5} \times 100\% \quad (1)$$

where C_i is the molar concentration of a particular compound. Whereas C_1, C_2, C_3, C_4 and iC_5 are the molar concentrations of methane, ethane, propane, butane and *iso*-pentane, respectively.

The specific rate of *n*-pentane conversion ($r_{n\text{-pentane}}$) from the differential conversion data was determined by Eq. (2)

$$r_{n\text{-pentane}} = k\frac{c_1 + c_2 + c_3 + c_4 + ic_5}{c_1 + c_2 + c_3 + c_4 + ic_5 + c_{5(res)}} \quad (2)$$

where the rate constant (k) was determined by the molar concentration of *n*-pentane divided by the surface area of catalyst per unit time. $C_{5(res)}$ represented the molar concentration of residual *n*-pentane in the product mixture. In this experiment, k was 2.89×10^{-7} mol s^{-1} m^{-2}-cat, with the assumption that the retention time for *n*-pentane in the catalyst bed was negligibly small.

3. Results and discussion

3.1. Structural properties of HZSM-5 and Zn/HZSM-5

Fig. 1 shows the XRD pattern of HZSM-5 and Zn/HZSM-5, confirming that the loading of Zn^{2+} does not change the peak position of parent HZSM-5. Physicochemical analysis by N_2 adsorption–desorption isotherms revealed that the BET specific surface areas of HZSM-5 and Zn/HZSM-5 were slightly different (511 and 495 m^2/g, respectively). The small decrease in the BET specific surface area of HZSM-5 was due to the 5 wt% loading of

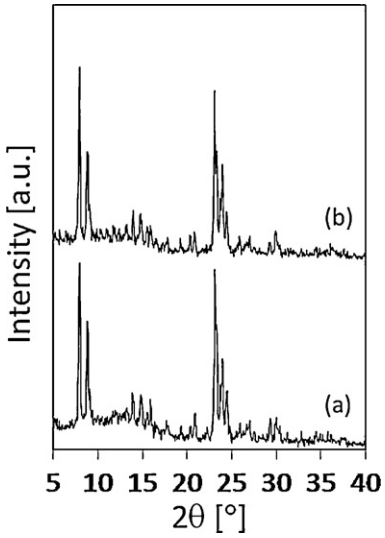

Fig. 1. XRD patterns of (a) HZSM-5 and (b) Zn/HZSM-5.

the zinc particles and not from the change and/or collapse of the crystalline framework. The absence of peaks ascribed to the ZnO particles at 2θ = 31.8, 34.5, 36.3, 47.6, 56.6, 62.9, 66.6, 67.9 and 69.1 (JCPDS file No. 36-1451) may have been caused by the absence of ZnO on the surface and/or inside the channel of the HZSM-5 framework. X-ray photoelectron spectroscopy (XPS) results confirmed the absence of zinc metal and ZnO. Fig. 2 shows the intensity of peaks at 531.1 and 1022.7 eV due to the O (1s) and Zn ($2p_{3/2}$) binding energy for $Zn^{2+}(O^-)_2$, whereas the Zn ($2p_{3/2}$) peaks correspond to Zn and ZnO are presumed at the lower binding energy range of 1021.5–1022.1 eV [38].

Fig. 3 shows the TEM micrographs of ZnO particle and Zn/HZSM-5. Single and aggregation of ZnO particles were shown in Fig. 3(A) and (B), whereas the HRTEM of ZnO particle and $Zn^{2+}(O^-)_2$ in the HZSM-5 were shown in Fig. 3(C) and (D). The insets showed corresponding selected-area electron diffraction patterns of ZnO and $Zn^{2+}(O^-)_2$ in HZSM-5. The images confirmed the size of both zinc oxide species was range from 10 to 15 nm. Therefore, it is suggested that the $Zn^{2+}(O^-)_2$ was located on the surface and/or pore mouth of HZSM-5 due to the size of zinc oxide species is bigger than the average pore size of HZSM-5. Moreover the introduction of Zn^{2+} did not change the surface are of HZSM-5 indicated that Zn^{2+} did not blockage the pore of HZSM-5. Fig. 4 shows the results of the SEM images and EDX analyses. The EDX analyses confirmed that no other metal was observed in the sample except for Zn and Pt. The presence of Pt was due to the sample preparation using a Pt sputtering instrument, which is a standard procedure for SEM observations. The high purity of the zinc particles provided for a BET specific surface area of 62 m^2/g.

3.2. Nature and strength of the acidity in HZSM-5 and Zn/HZSM-5

3.2.1. Probing by pyridine adsorption

The type of acid sites in HZSM-5 and Zn/HZSM-5 was qualitatively probed by pyridine adsorption using IR spectroscopy. Fig. 5 shows the IR spectra of activated HZSM-5 and Zn/HZSM-5 after outgassing at 623 K for 3 h prior to pyridine adsorption. Fig. 6 shows IR spectra of adsorbed pyridine on HZSM-5 and Zn/HZSM-5 samples. These spectra were recorded after the adsorption of pyridine on samples reach equilibrium at 423 K and the physisorbed state was subsequently removed by heating at 598 K under vacuum. The resulting bands indicated only strong adsorption between the pyridine molecules and zeolite active sites. Typical Brønsted acid sites formed by bridging hydroxyl groups (SiOHAl groups) were observed in the HZSM-5 sample, suggesting that pyridine was adsorbed in the form of a pyridinium ion at the IR frequency of 1545 cm^{-1}. However, no significant Lewis acidic group was found at 1454 cm^{-1} in the parent zeolite. Therefore, the coordinative Al^{3+} cations located in the extra framework Al-oxide cluster act as very weak Lewis electron pair acceptor. The band at 1490 cm^{-1} corresponds to the mixture of Brønsted and Lewis acid sites. The introduction of Zn^{2+} on HZSM-5 replaces the acidic hydroxyl groups

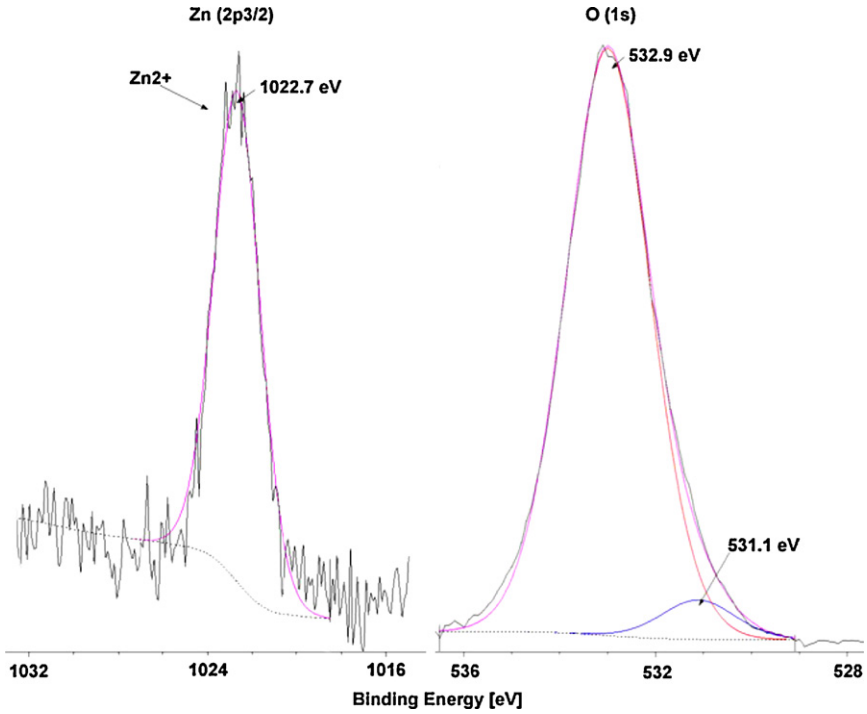

Fig. 2. XPS spectra at 531.1 and 1022.7 eV due to the O (1s) and Zn ($2p_{3/2}$) binding energy for $Zn^{2+}(O^-)_2$.

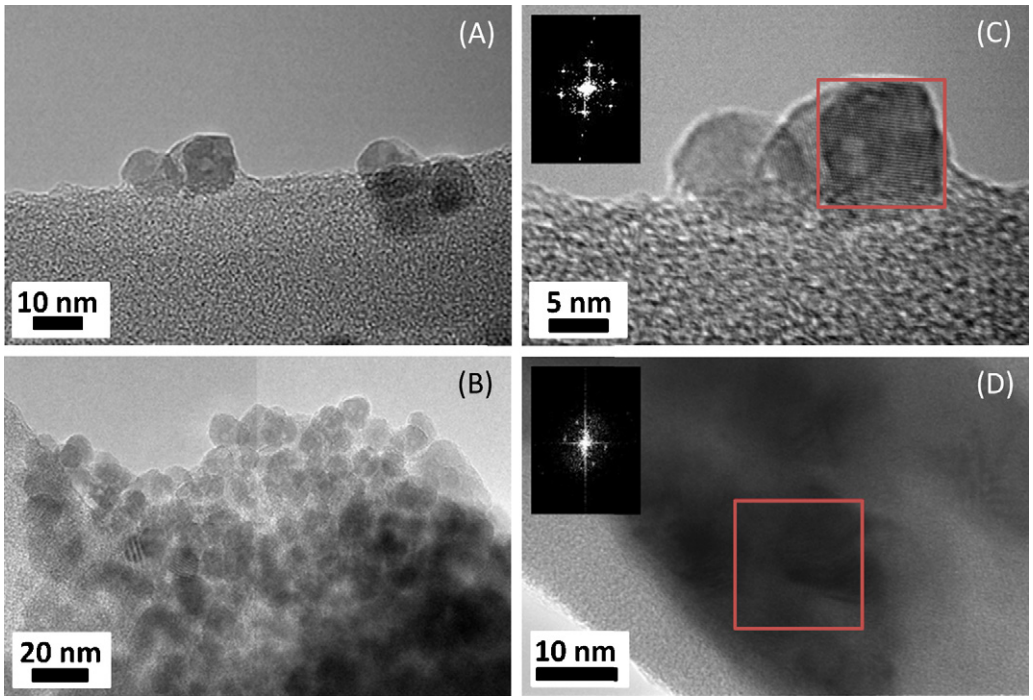

Fig. 3. TEM micrographs of ZnO particle and Zn/HZSM-5 sample. (A) single and (B) aggregation of ZnO particle. (C) and (D) are HRTEM of ZnO particle and Zn/HZSM-5. Insets show the selected-area electron diffractions. Locus of the performed electron diffractions analysis is shown by red square.

Si(OH)Al and forms Lewis acid sites ($Zn^{2+}(O^-)_2$). The intensity of peaks at 3610, 1545 and 1490 cm^{-1} decreased, whereas the peak intensity at 1454 cm^{-1} markedly increased. The exchange of acidic character revealed that impregnation of the Zn^{2+} may partially eliminate the Brønsted acid sites and induce the generation of Lewis acid sites. Based on the XPS results and previous reports [32], the active Zn species in HZSM-5 serving as Lewis acids can be suggested in at least two $Zn^{2+}(O^-)_2$ structures: one Zn^{2+} ion interacting with two cation-exchange sites (Al and Si) bridged by an oxygen and one Zn^{2+} ion interacting with two Zn^{2+} ions bridged by an oxygen.

The strength of the Brønsted and Lewis acid sites on Zn/HZSM-5 was investigated by outgassing of the preadsorbed pyridine sample at different temperatures (Fig. 7). As the outgassing temperature was raised, the Brønsted and Lewis acid sites bands were unchanged up to 598 K. Calculations of the fraction of acid sites showed almost constant values throughout heating (Fig. 7(B)). Both Brønsted and Lewis acid sites in Zn/HZSM-5 showed remarkable strength in the outgassing at 598 K and below. No acid strength distribution for both the Lewis and Brønsted acid sites was observed

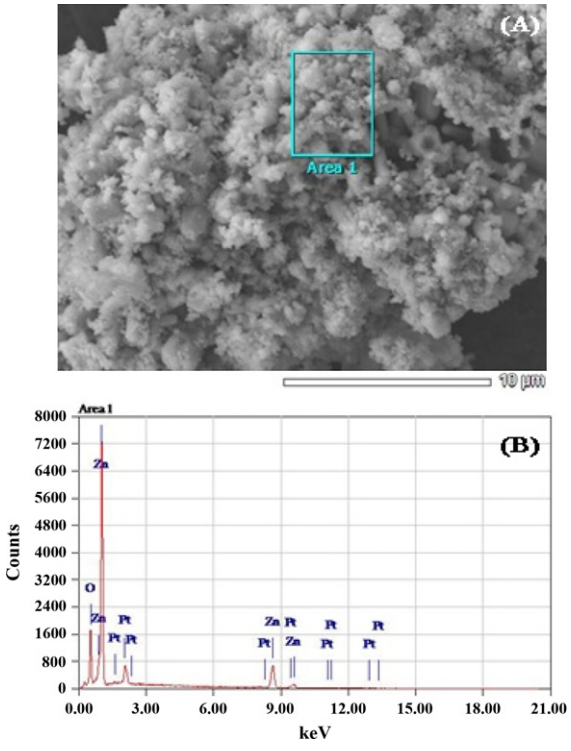

Fig. 4. (A) FESEM micrograph and (B) EDX analysis of powder form of zinc oxide particle. Locus of the performed EDX analysis is shown by box "Area 1".

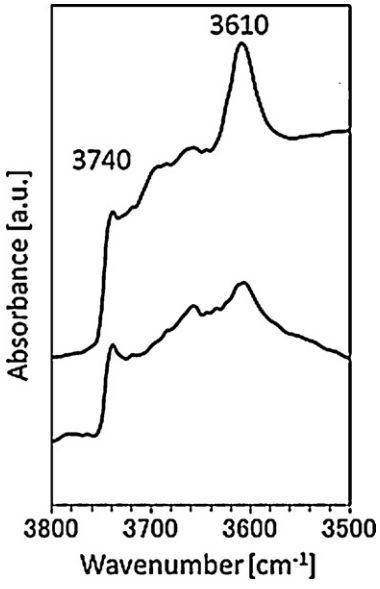

Fig. 5. IR spectra of activated (a) HZSM-5 and (b) Zn/HZSM-5.

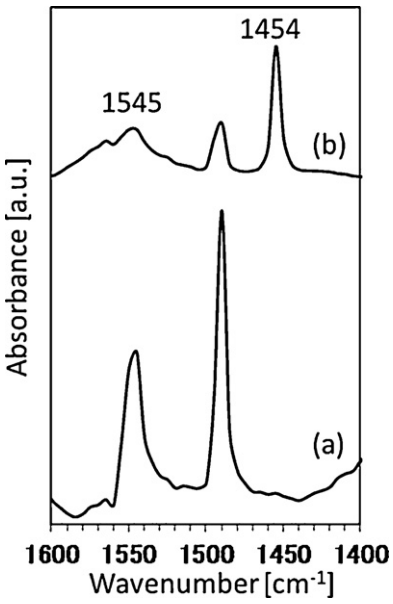

Fig. 6. IR spectra of pyridine adsorbed on activated (a) HZSM-5 and (b) Zn/HZSM-5 at 423 K followed by removal of pyridine at 598 K.

for this sample. The nature of the acidic sites on Zn/HZSM-5 is different from that of other solid acid catalysts based on ZrO_2 such as Pt/SO_4^{2-}-ZrO_2 and Pt/WO_3-ZrO_2 [4,19]. Pt/SO_4^{2-}-ZrO_2 and Pt/WO_3-ZrO_2 possess strong Brønsted and Lewis acid sites. In addition to strong Lewis acid sites, a considerable number of weak Lewis acid sites also exist on Pt/SO_4^{2-}-ZrO_2 and Pt/WO_3-ZrO_2.

3.2.2. Probing by ammonia adsorption

The pyridine molecule can be used to probe changes in the acidic character of HZSM-5 after the impregnation with zinc particles. To further clarify the nature and strength of the acidity, the adsorption of ammonia was measured. Fig. 8 shows the spectra of adsorbed ammonia on activated HZSM-5 and Zn/HZSM-5 after outgassing at 373 and 473 K. The absorption band at 1455 cm^{-1}, which was attributed to the ammonium ions (NH_4^+) bound on the Brønsted acid sites, was observed for both HZSM-5 and Zn/HZSM-5 [39]. For both samples, this band decreased slightly with increasing temperature during the outgassing period, emphasizing the remarkable

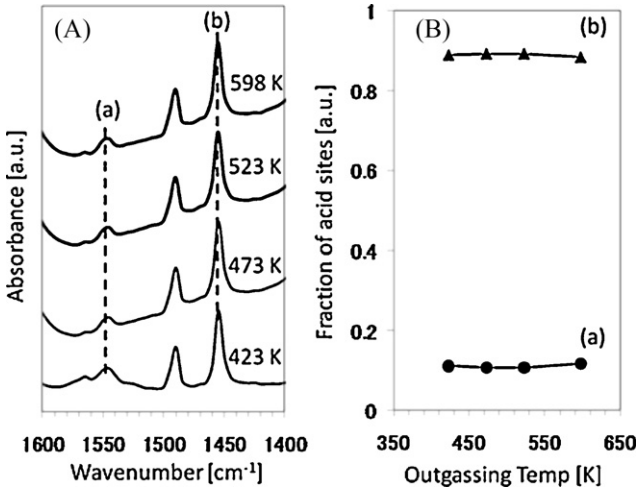

Fig. 7. (A) IR spectra of pyridine adsorbed on Zn/HZSM-5 pretreated at 623 K for 30 min followed by removal of pyridine at 423, 473, 523 and 598 K for 30 min, respectively. The spectra were taken at room temperature. (B) The fraction of acid sites after removal of pyridine at different temperature.

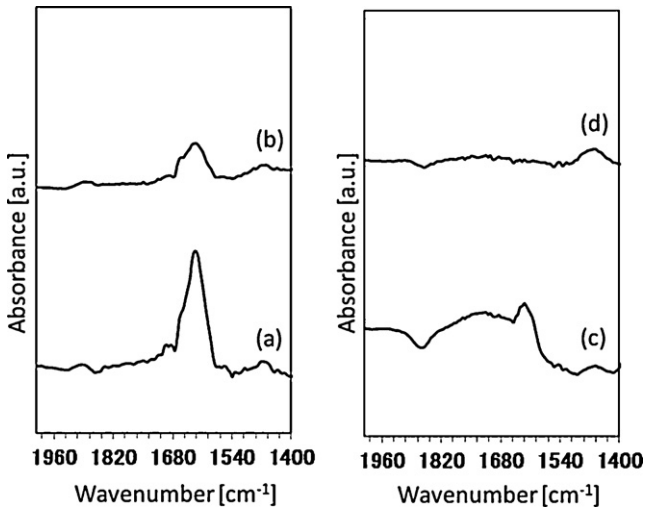

Fig. 8. IR spectra of ammonia adsorbed on (A) Zn/HZSM-5 and (B) HZSM-5 samples. Spectra (a) and (b) for ammonia adsorbed on Zn/HZSM-5 after outgassing at 373 and 473 K, respectively. Spectra (c) and (d) for ammonia adsorbed on HZSM-5 after outgassing at 373 and 473 K, respectively.

strength of Brønsted acid sites. This result is in line with the results from pyridine outgassing in a heated condition, as the intensity of the Brønsted peak is difficult to determine in these two samples. The Brønsted acidic groups are present only in a small fraction of the acid sites with respect to Lewis acidic groups, even though they are strong.

The Lewis acid sites are present in the absorption band that appears at 1625 cm^{-1}, which was more intense after exchange of the Zn^{2+} into HZSM-5. This band disappeared after outgassing at 473 K for the HZSM-5 sample, but only decreased to a lower concentration after outgassing at 473 K for the Zn/HZSM-5 sample. In addition, a new broadened band at 1890 cm^{-1} with shoulders at 1660 and 1685 cm^{-1} were generated with Zn/HZSM-5. These bands indicated interactions between ammonia species and several types of Lewis acid sites provided by the Zn^{2+} cation exchanged in zeolite. An adequate intensity of the peaks was observed after outgassing at 473 K, revealing the presence of strong Lewis acidic groups in Zn/HZSM-5. These results are in agreement with the exchanged acidic character in the Zn-impregnated HZSM-5.

3.2.3. Probing by carbon monoxide adsorption

Strong bases, such as pyridine, can be used to probe the Brønsted and Lewis acidic groups of 10-membered ring zeolites such as ZSM-5 (MFI structure). Small and weak electron-donating molecules, such as carbon monoxide, can also be used as probe molecules to characterize these acidic groups. Carbon monoxide may form H bonds with the hydroxyl groups, which can be easily observed with IR spectroscopy by following the absorption in the OH and CO stretching regions. When adsorbing CO on zeolite, the frequency of the CO stretching vibrations increases along with a simultaneous decrease in the frequency of the OH stretching vibrations. Fig. 9 shows that CO can be adsorbed on Zn/HZSM-5, with the formation of a distinct band at 2158 cm^{-1} and very weak bands around 2132 cm^{-1}. By contrast, no bands were observed in the frequency range of 2185–2200 cm^{-1} for HZSM-5. The absence of a gas phase frequency at 2143 cm^{-1} (physisorption) and of the H bond frequency in the carbonyl stretching region at 2173 cm^{-1} (chemisorption) further suggest that the CO molecules were not introduced in a high concentration under the current experimental conditions (P_{CO} = 2 Torr at room temperature). Normally, such CO uptake can be enhanced if liquid nitrogen temperatures are used [40]. Nevertheless, we were able to observe the difference

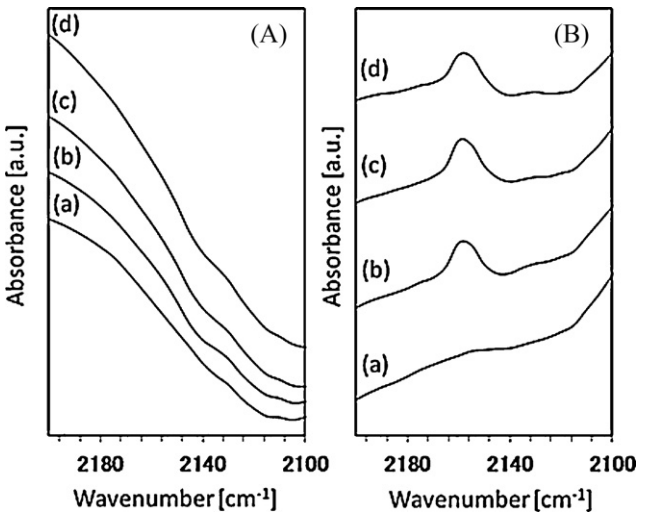

Fig. 9. IR spectra of CO adsorbed on activated (A) HZSM-5 and (B) Zn/HZSM-5 at room temperature. (a) Before adsorption of CO; (b) immediately after admission of CO; after (c) 10 and (d) 30 min of CO admission at room temperature.

between HZSM-5 and Zn/HZSM-5 with the current conditions. The distinct peaks at 2158 cm^{-1} can likely be attributed to the monocarbonyl formed due to the Zn^{2+}, while the very weak band around 2132 cm^{-1} may be associated with the monocarbonyl adsorbed on the surface defect caused by the presence of zinc species and/or bulk zinc oxide particles [41]. The intensity of these bands did not change after 30 min of CO exposure, indicating that the Lewis acid sites on Zn/HZSM-5 are strong acidic groups.

Many studies have reported the promotive effect of Zn species on ZSM-5 by several preparation methods employing various ionic forms of ZSM-5 (e.g. NH_4^+) and Zn precursors. For example, $Zn(NO_3)_2{\cdot}6H_2O$ [39], $ZnCl_2$ [42] and $Zn(NO_3)_2$ solutions [32] have been implemented by reflux, chemical vapor deposition and ion exchange, respectively. In all of these examples, the Lewis acidic groups are generated along with the elimination of the Brønsted acidic groups, in accordance with the current investigation using the Zn^{2+}/N,N-dimethylformamide solution as the zinc particle precursor for the HZSM-5. Although H-bonded complexes (Brønsted acid site) were not observed during CO adsorption, the presence of Lewis acidic groups has clearly been demonstrated in Zn/HZSM-5 and may support the exchanged acidic character with impregnation of zinc particles in HZSM-5.

3.3. Hydrogen spillover behavior in Zn/HZSM-5

The probability of hydrogen spillover onto the surface of Zn-impregnated zeolite in the presence of hydrogen was investigated. Pyridine was used as a probe molecule to study the evolution of Brønsted acidic groups on Zn/HZSM-5. The Lewis acidic groups were expected to decrease as a consequence of molecular hydrogen addition.

Results from IR spectroscopy revealed a relatively small concentration of Brønsted acid sites in Zn/HZSM-5, which were observed in the form of pyridinium ions at 1545 cm^{-1} and dominant Lewis acid sites at 1454 cm^{-1} (see Section 3.2.1). Subsequently, hydrogen was introduced into pyridine-adsorbed Zn/HZSM-5, and the system was heated at 298, 323, 348, 373 and 398 K. The spectra shown in Fig. 10 had the spectrum prior to the hydrogen addition subtracted from them, so the effect of hydrogen in the pyridine-adsorbed sample could be clearly observed. These spectra systematically portray an increase of the Brønsted acid sites and a concomitant decrease of the Lewis acid sites, which corresponds to hydrogen spillover as the function of temperature. The fraction of acid sites was calculated, showing a clear switch of acidic character during the hydrogen spillover (Fig. 10(C)). We interpreted this result as the formation of protonic acid sites after the addition of hydrogen and a simultaneous decrease in the number of Lewis acid sites. By switching the acidic character from Lewis to protonic acid sites, Zn/HZSM-5 can perform the hydrogen spillover behavior.

To investigate the strength of the formed protonic acid sites, the sample was heated under vacuum. The protonic acid sites remained stable up to 348 K, but the Lewis acid sites had just started to evolve. By further heating, the acidic character eventually switched back to the initial state where the Brønsted acid sites were at a relatively small concentration and the Lewis acid sites dominated. These results showed that the hydrogen spillover phenomenon is a reversible process (Fig. 11). The calculated fraction of acid sites showed a gradual character switch from predominately protonic acid sites back to Lewis acid sites.

The generation of protonic acid sites from hydrogen molecules could not be observed on HZSM-5 (not shown), which may be due

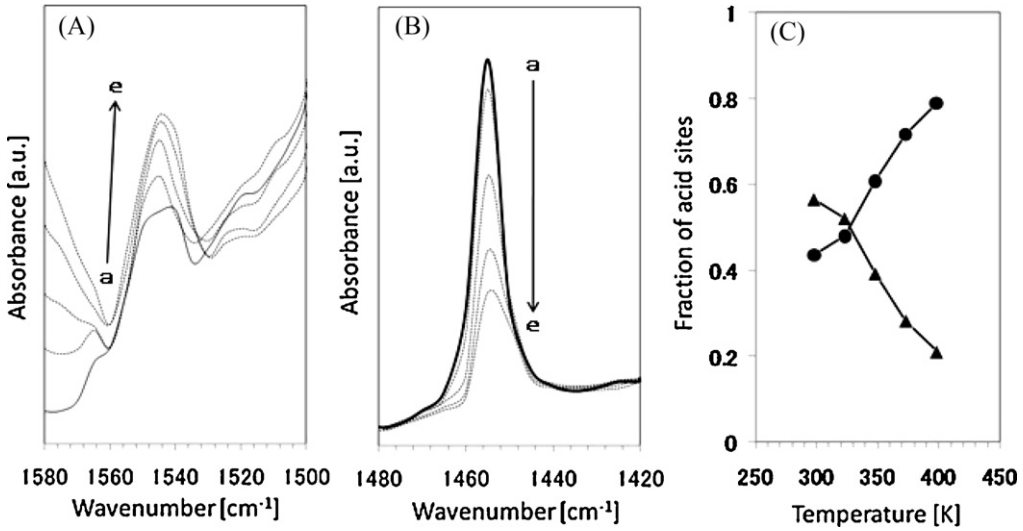

Fig. 10. IR spectra of pyridine adsorbed on Zn/HZSM-5. Spectral changes when pyridine-preadsorbed sample was heated in hydrogen at (a) 298 K, (b) 323 K, (c) 348 K, (d) 373 K and (e) 398 K. The spectra were taken at room temperature. (C) The fraction of acid sites after heating in the presence of hydrogen at different temperatures. Triangle and circle are Lewis and protonic acid sites at room temperature, respectively.

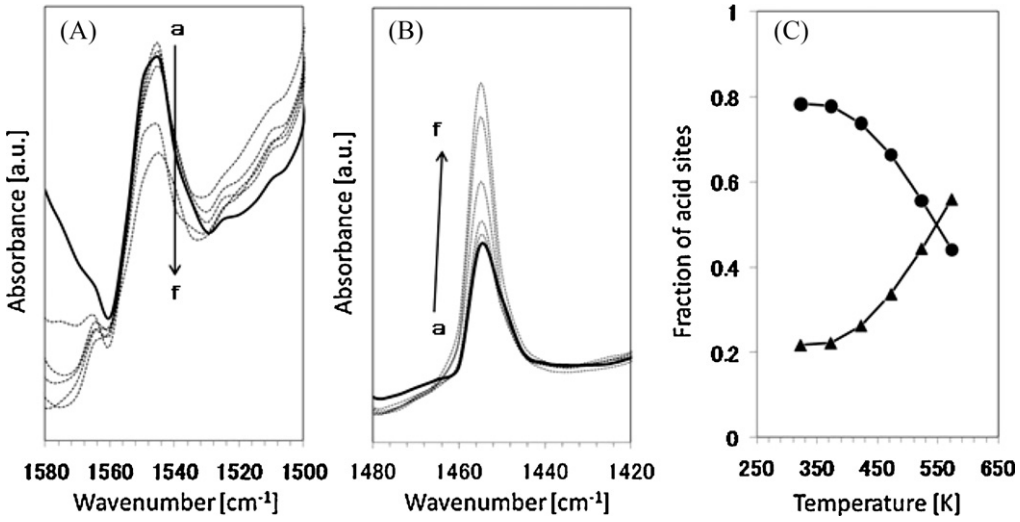

Fig. 11. The change of spectrum (e) in Fig. 10 when hydrogen was removed at (a) 323 K, (b) 373 K, (c) 423 K, (d) 473 K, (e) 523 K and (f) 573 K. The spectra were taken at room temperature. (C) The fraction of acid sites after removal of hydrogen at different temperatures. Triangle and circle are Lewis and protonic acid sites at room temperature, respectively.

to the absence of Lewis acid sites within the sample. Specific active sites such as Lewis acid sites are necessary to facilitate the dissociation of molecular hydrogen to hydrogen atoms, which is mediated by metal and acidic oxide supports. Although there are some differences, the phenomena observed on Zn/HZSM-5 are essentially the same as those observed for SO_4^{2-}-ZrO_2 and WO_3-ZrO_2 catalysts, which follow the concept of 'molecular hydrogen-originated protonic acid sites' [3,8,43]. Metal species are required for the formation of protonic acid sites from hydrogen molecules for SO_4^{2-}-ZrO_2 and HZSM-5, but are not necessary for WO_3-ZrO_2. The other difference is the ease of conversion of Lewis acid sites to protonic acid sites. The conversion was appreciable at 473 K for Pt/SO_4^{2-}-ZrO_2 but could not be observed for Pt-free SO_4^{2-}-ZrO_2. However, the conversion was observed at near room temperature and 373 K for WO_3-ZrO_2 with and without Pt, respectively. In this study, the conversion of Lewis acid sites to protonic acid sites on Zn/HZSM-5 was observed at room temperature and above. The ease of generating protonic acid sites on Zn/HZSM-5 may be due to the presence of strong Lewis acid sites and zinc particles. These results indicate that the specific active sites such as zinc particles and strong Lewis acid sites are pre-requisites for the generation of protonic acid sites on HZMS-5. The zinc particles may act as an active site for the dissociation of molecular hydrogen into hydrogen atoms and the Lewis acid sites may stabilize protons by accepting electrons from hydrogen atoms.

The non-dissociative adsorption of hydrogen on Zn/HZSM-5 at low temperature was reported by Kazansky et al. [44] using the DRIFT method. Zn/HZSM-5 was prepared by impregnation of NH_4ZSM-5 with zinc nitrate followed by high-temperature treatment. The adsorption of molecular hydrogen on HZSM-5 and Zn/HZSM-5 led to the development of bands at 4105, 4125 and 4180 cm^{-1}, which were ascribed to the stretching vibrations of hydrogen adsorption on acidic hydroxyls and silanol groups. The presence of Zn on HZSM-5 generated new bands at 3940, 4005 and 4030 cm^{-1}, which were attributed to molecular hydrogen adsorbed on Lewis acid sites with various strengths connected with coordinatively unsaturated Zn^{2+} cations. The dissociative-adsorption of molecular hydrogen occurs at room and elevated temperatures on Zn/HZSM-5 due to the presence of strong Lewis acid sites. The band at 3940 cm^{-1} may correspond to the presence of zinc oxide nanometric clusters in the channels of the zeolite framework. The presence of Lewis acid sites with different strengths on Zn/HZSM-5 determined with DRIFT using hydrogen as a probe molecule is in accordance with transmission IR observations using ammonia as a probe molecule.

3.4. Hydrogenation of chemisorbed pyridine

Fig. 12 shows IR spectral changes for pyridine adsorbed on Zn/HZSM-5 at room temperature, 348, 523 and 573 K under 50 Torr of hydrogen. With heating at 348 K, the intensity of the bands at 1545 and 1490 cm^{-1} increased, whereas the intensity of the band at 1454 cm^{-1} decreased. With heating at 523 K, a new IR band appeared at 1470 cm^{-1} with a concomitant decrease in the intensity of the bands at 1490, 1454 and 1545 cm^{-1}. This new band is associated with adsorbed piperidine [4] and the intensity further increased at 573 K. In the presence of hydrogen above 523 K, the

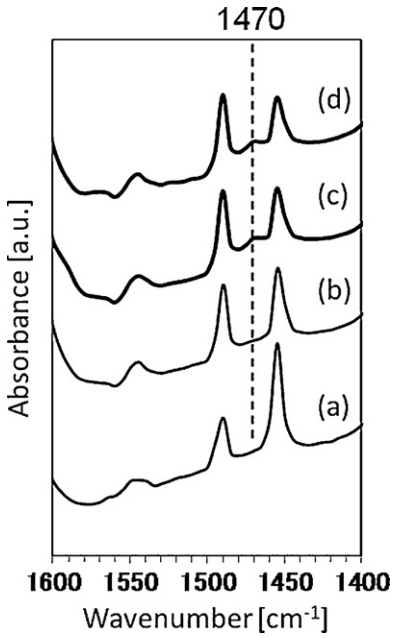

Fig. 12. Hydrogenation of pyridine adsorbed on Zn/HZSM-5 at (a) room temperature, (b) 348 K, (c) 523 K and (d) 573 K under 20 kPa of hydrogen. The heating was carried out for 15 min for each temperature. The spectra were taken at room temperature.

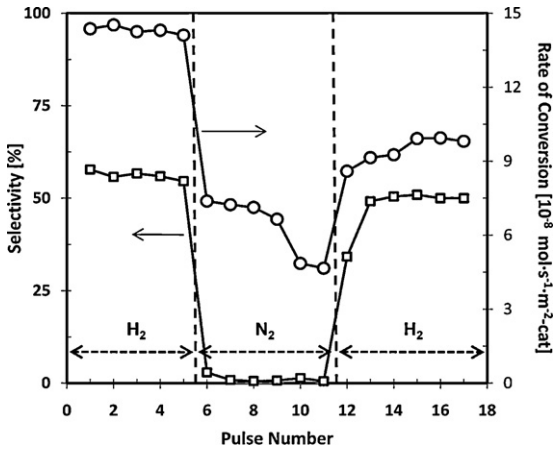

Fig. 13. Effect of carrier gases in the selectivity and rate conversion for isomerization of *n*-pentane at 523 K over Zn/HZSM-5.

adsorption of pyridine on both protonic and Lewis acid sites of Zn/HZSM-5 resulted in hydrogenation of chemisorbed pyridine.

Zhang et al. [26] reported the hydrogenation of chemisorbed pyridine on Pt/HZSM-5 at 473 K. The chemisorbed pyridine was converted into piperidine after exposing the catalyst with 40 kPa of hydrogen for 1 h. However, we could not observe the formation of piperidine on Zn/HZSM-5 at 473 K or lower. The different hydrogenation temperatures may be caused by differences in the partial pressure of hydrogen or in the ability of the catalysts to dissociate molecular hydrogen-to-hydrogen atoms. We have also reported the hydrogenation of chemisorbed pyridine on a WO_3-ZrO_2-type catalyst [4]. At 373 K, hydrogenation occurred for Pt-loaded WO_3-ZrO_2 whereas no hydrogenation occurred for Pt-free WO_3-ZrO_2. The formation of protonic acid sites caused the distinct behavior in which Pt-loaded WO_3-ZrO_2 formed protonic acid sites at room temperature whereas Pt-free WO_3-ZrO_2 only developed protonic acid sites at 373 K.

3.5. Isomerization of n-pentane

Figs. 13 and 14 show the isomerization of *n*-pentane on Zn/HZSM-5 and the distribution of the cracking products at 523 K in a microcatalytic pulse reactor. The outlet was composed of *iso*-pentane, cracking products (C_1, C_2, C_3 and C_4) and residual

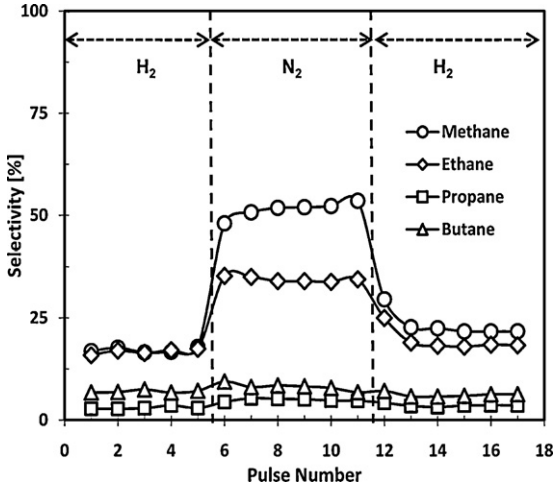

Fig. 14. Effect of carrier gases in the selectivity to cracking-products (C_1–C_4) for isomerization of *n*-pentane at 523 K over Zn/HZSM-5.

n-pentane, but no C_6 and/or higher hydrocarbon was formed. In this experiment, the carrier gas was sequentially switched from hydrogen to nitrogen and switched back to hydrogen in order to examine the promotive effect of hydrogen on Zn/HZSM-5 catalysis. The presence of zinc particles resulted in a substantial increase in activity and stability of HZSM-5 for the isomerization of *n*-pentane. Moreover, the presence of molecular hydrogen on specific active species, such as zinc species, may contribute to inhibition of coke formation on the catalyst surface. Although not shown here, *n*-pentane isomerization was not appreciable with the powder form of the ZnO particle (selectivity: 0%, conversion < 1%) and Zn-free HZSM-5 catalyst (selectivity: 7.4%, conversion < 3%) regardless of the carrier gases used. The lack of activity is caused by the inability of the catalyst to generate protonic acid sites from molecular hydrogen as the catalytically active sites.

In the first five doses under a hydrogen stream, Zn/HZSM-5 exhibited high activity and stability for *n*-pentane isomerization. The selectivity of Zn/HZSM-5 for *iso*-pentane and the rate of *n*-pentane conversion were about 55% and 14.4×10^{-8} mol s^{-1} m^{-2}-cat, respectively. The rate of *n*-pentane conversion decreased by half when the carrier gas of hydrogen was switched to nitrogen (Fig. 13). The rate of *n*-pentane conversion decreased continuously with the pulse number and reached 4.65×10^{-8} mol s^{-1} m^{-2}-cat at the sixth dose in a nitrogen stream. The selectivity to *iso*-pentane was close to zero for the isomerization in a nitrogen stream. The decreased catalytic activity after switching the carrier gas to nitrogen was due to the gradual exhaustion of adsorbed hydrogen (protonic acid cites) on the surface of the catalyst. The absence of molecular hydrogen may prevent the formation of protonic acid sites, resulting in the inhibition of isomerization. At this state, the Lewis acid sites may be restored to their original strength.

The activity and stability of Zn/HZSM-5 recovered slowly with the pulse number when the carrier gas was switched back to the hydrogen. The selectivity to *iso*-pentane was almost recovered to the initial condition but the rate of *n*-pentane conversion dropped by 30% to ca. 9.9×10^{-8} mol s^{-1} m^{-2}-cat. Although the activity and stability did not recover completely after switching back to the hydrogen, the promoting effect of hydrogen was observed on the Zn/HZSM-5 catalyst. Deactivation of Zn/HZSM-5 may be caused by the formation of coke deposits on the surface of Zn/HZSM-5 during the reaction in a nitrogen stream. Even though the mechanism of coke formation over Zn/HZSM-5 is not yet clear, strong Lewis acid sites in the absence of hydrogen may become active sites for the formation of dehydrogenated carbonaceous species, which are considered to be a precursor of coke on the catalyst surface [6]. These results helped us to understand why the dehydrogenated carbonaceous species was relatively easy to form in the absence of hydrogen.

The distribution of cracking products is shown in Fig. 14 and Table 1. The formation of C_1–C_2 quickly increased the selectivity from 35.3 to about 86.1% when the carrier gas of hydrogen was switched to nitrogen. The selectivity to C_1 increased continuously with the pulse number, while the selectivity to C_2 was almost constant at about 35% for the isomerization in a nitrogen stream. The selectivity of C_1–C_2 decreased to about 40% when the carrier gas was switched back to hydrogen gas. The selectivity to C_3–C_4 was about 10% and had no significant effect with the carrier gas switching. The promotive effects of hydrogen were observed in the formation of *iso*-pentane and in the suppression of C_1–C_2 cracking products over Zn/HZSM-5 catalyst. Removal of the hydrogen stream may cause a decrease in the activity and stability of the Zn/HZSM-5 catalyst.

The promotive effects of hydrogen on the hydrocarbon isomerization or cracking over Pt/SiO_2 and protonated zeolitic materials were reported by Fujimoto et al. [2]. They discussed that the participation of H^+ and H^- was initiated by dissociative adsorption

Table 1
Effect of carrier gas on rate conversion of *n*-pentane and product selectivity for Zn/HZSM-5 catalyst at 523 K. A number in the parenthese indicated the product for the isomerization over Zn-free HZSM-5.

	Carrier gas		
	1st cycle hydrogen[a]	2nd cycle nitrogen[a]	3rd cycle hydrogen[a]
Rate Conversion [mol s^{-1} m^{-2}-cat]	14.1×10^{-8}	$4.9 \times 10^{-8}(8.7 \times 10^{-9})$	9.9×10^{-8}
Selectivity [%]:			
C_1–C_2	35.3(78.7)	86.1	40.1
C_3–C_4	10.1(13.9)	12.6	9.7
Iso-pentane	54.6(7.4)	1.3	50.2

[a] Fifth dose data after switching of the carrier gas.

of hydrogen on a metal followed by spillover of a hydrogen atom to support the acidic center. Shishido and Hattori [6] reported the promotive effects of hydrogen on cumene cracking over Pt/SO_4^{2-}-ZrO_2. The presence of hydrogen enhanced the activity and stability of the Zn/HZSM-5 catalyst by forming the protonic acid sites. Moreover, it also suppressed the formation of coke. No promotive effect of hydrogen was observed on the Pt-free SO_4^{2-}-ZrO_2 or sulfate ion-free Pt/ZrO_2 catalysts.

4. Conclusions

In the presence of hydrogen, zinc particles impregnated on HZSM-5 can be used as a solid acid catalyst due to catalytically active protonic acid sites formed via the hydrogen spillover mechanism. An IR study of adsorbed pyridine revealed that the formation of protonic acid sites on Zn/HZSM-5 is a reversible process. In contrast to Zn/HZSM-5, unmodified HZSM-5 did not exhibit any hydrogen spillover behavior. Based on the preadsorbed pyridine, ammonia and carbon monoxide IR studies, impregnation of Zn particles on HZSM-5 led to the exchange of the acidic characters of HZSM-5. The Brønsted acid sites were eliminated with simultaneous formation of strong Lewis acid sites. In contrast, unmodified HZSM-5 possesses only Brønsted acid sites. Therefore, the hydrogen spillover behavior of Zn/HZSM-5 occurs due to the presence of strong Lewis acid sites derived from the zinc species exchanging with the surface OH to form $Zn^{2+}(O^-)_2$. Notably, the presence of zinc species on HZSM-5 did not change the structural characteristics of HZSM-5. The isomerization of *n*-pentane over Zn/HZSM-5 using hydrogen as a carrier gas resulted in a high catalytic activity and catalyst stability. The conversion to *iso*-pentane decreased when the carrier gas was switched from hydrogen to nitrogen. Consequently, the formation of cracking products markedly increased. By switching back the carrier gas to hydrogen, the activity of Zn/HZSM-5 returned. Therefore, the high catalytic activity in the isomerization of *n*-pentane over this solid super acid catalyst is strongly determined by the presence of catalytically active protonic acid sites.

Acknowledgements

This work was supported by the Ministry of Science, Technology and Innovation, Malaysia (MOSTI) under E-Science Fund Research Projects No. 03-01-06-SF0020 and 03-01-06-SF0564. Our gratitude also goes to the Hitachi Scholarship Foundation for the Gas Chromatograph Instruments Grant and Center for Research and Instrumentation Management (CRIM, UKM) for the XPS data and analysis.

References

[1] A.H. Zhang, I. Nakamura, K. Aimoto, K. Fujimoto, Ind. Eng. Chem. Res. 34 (1995) 1074–1080.
[2] K. Fujimoto, K. Maeda, K. Aimoto, Appl. Catal. A 91 (1992) 81–86.
[3] S. Triwahyono, T. Yamada, H. Hattori, Appl. Catal. A 250 (2003) 75–81.
[4] S. Triwahyono, T. Yamada, H. Hattori, Appl. Catal. A 242 (2003) 101–109.
[5] S. Triwahyono, A.A. Jalil, M. Musthofa, Appl. Catal. A 372 (2010) 90–93.
[6] T. Shishido, H. Hattori, J. Catal. 161 (1996) 194–197.
[7] T. Shishido, H. Hattori, Appl. Catal. A 146 (1996) 157–164.
[8] K. Ebitani, J. Tsuji, H. Hattori, H. Kita, J. Catal. 135 (1992) 609–617.
[9] W.C. Conner, J.L. Falconer, Chem. Rev. 95 (1995) 759–788.
[10] S. Triwahyono, A.A. Jalil, H. Hattori, J. Nat. Gas Chem. 16 (2007) 252–257.
[11] T. Kusakari, K. Tomishige, K. Fujimoto, Appl. Catal. A 224 (2002) 219–228.
[12] F. Roessner, U. Roland, J. Mol. Catal. A 112 (1996) 401–412.
[13] N. Essayem, Y.B. Taarit, C. Feche, P.Y. Gayraud, G. Sapaly, C. Naccache, J. Catal. 219 (2003) 97–106.
[14] S. Kuba, P. Lukinskas, R.K. Grasselli, B.C. Gates, H. Knözinger, J. Catal. 216 (2003) 353–361.
[15] S. Kuba, P. Lukinskas, R. Ahmad, F.C. Jentoft, R.K. Grasselli, B.C. Gates, H. Knözinger, J. Catal. 219 (2003) 376–388.
[16] M.F. Williams, B. Fonfé, C. Woltz, A. Jentys, J.A.R. van Veen, J.A. Lercher, J. Catal. 251 (2007) 497–506.
[17] E. Iglesia, S.L. Soled, G.M. Kramer, J. Catal. 144 (1993) 238–253.
[18] P.B. Weisz, E.W. Swegler, Science 126 (1957) 31–32.
[19] S. Triwahyono, Z. Abdullah, A.A. Jalil, J. Nat. Gas Chem. 15 (2006) 247–252.
[20] C. Woltz, A. Jentys, J.A. Lercher, J. Catal. 237 (2006) 337–348.
[21] Y. Ono, Catal. Today 81 (2003) 3–16.
[22] A. Corma, J. Catal. 216 (2003) 298–312.
[23] A. Corma, Chem. Rev. 97 (1997) 2373–2419.
[24] M.E. Davis, R.F. Lobo, Chem. Mater. 4 (1992) 756–768.
[25] M.E. Davis, Ind. Eng. Chem. Res. 30 (1991) 1675–1683.
[26] A.H. Zhang, I. Nakamura, K. Fujimoto, J. Catal. 168 (1997) 328–333.
[27] H. Yang, H. Chen, J. Chen, O. Omotoso, Z. Ring, J. Catal. 243 (2006) 36–42.
[28] R. Ueda, K. Tomishige, K. Fujimoto, Catal. Lett. 57 (1999) 145–149.
[29] R. Ueda, T. Kusakari, K. Tomishige, K. Fujimoto, J. Catal. 194 (2000) 14–22.
[30] A. Chica, A. Corma, J. Catal. 187 (1999) 167–176.
[31] J.A. Biscardi, E. Iglesia, J. Catal. 182 (1999) 117–128.
[32] J.A. Biscardi, G.D. Meitzner, E. Iglesia, J. Catal. 179 (1998) 192–202.
[33] A.A. Jalil, N. Kurono, M. Tokuda, Tetrahedron 58 (2002) 7477–7484.
[34] S. Triwahyono, T. Yamada, H. Hattori, Catal. Lett. 85 (2003) 109–115.
[35] A. Jentys, R.R. Mukti, H. Tanaka, J.A. Lercher, Microporous Mesoporous Mater. 90 (2006) 284–292.
[36] R.R. Mukti, A. Jentys, J.A. Lercher, J. Phys. Chem. C 111 (2007) 3973–3980.
[37] M.F. Williams, B. Fonfé, C. Sievers, A. Abraham, J.A. van Bokhoven, A. Jentys, J.A.R. van Veen, J.A. Lercher, J. Catal. 251 (2007) 485–496.
[38] S. Hashimoto, M. Abe, Corros. Sci. 36 (1994) 2125–2137.
[39] H. Berndt, G. Lietz, B. Lücke, J. Völter, Appl. Catal. A 146 (1996) 351–363.
[40] Z. Schay, H. Knözinger, L. Guczi, G. Pál-Borbély, Appl. Catal. B 18 (1998) 263–271.
[41] T. Venkov, K. Hadjiivanov, Catal. Commun. 4 (2003) 209–213.
[42] E.M. El-Malki, R.A. van Santen, W.M.H. Sachtler, J. Phys. Chem. B 103 (1999) 4611–4622.
[43] S. Triwahyono, T. Yamada, H. Hattori, Catal. Appl. A 250 (2003) 65–73.
[44] V.B. Kazansky, V.Yu. Borokov, A.I. Serikh, R.A. van Santen, B.G. Anderson, Catal. Lett. 66 (2000) 39–47.